Materials Letters 212 (2018) 51–53

Contents lists available at ScienceDirect

Materials Letters

journal homepage: www.elsevier.com/locate/mlblue

MBE growth and morphology control of ZnO nanobelts with polar axis perpendicular to growth direction

Oscar W. Kennedy [a,b,*], Maddison L. Coke [a,b], Edward R. White [c], Milo S.P. Shaffer [c], Paul A. Warburton [a,b,*]

[a] London Centre for Nanotechnology, University College London, London WC1H 0AH, United Kingdom
[b] Department of Electronic and Electrical Engineering, University College London, London WC1E 7JE, United Kingdom
[c] Department of Chemistry, Imperial College London, London SW7 2AZ, United Kingdom

ARTICLE INFO

Article history:
Received 20 September 2017
Received in revised form 3 October 2017
Accepted 4 October 2017
Available online 5 October 2017

Keywords:
MBE
Zinc oxide
Nanowires
Nanobelts

ABSTRACT

In quasi-one-dimensional polar nanostructures the relative orientation of the long and polar axes will determine how the polarity of the nanostructure may be exploited for applications. Here we present the growth by molecular-beam epitaxy of quasi-1d ZnO nanostructures (specifically nanobelts) with the polar axis perpendicular to the growth axis. We demonstrate the control of nanostructure morphology by growth temperature. Our work represents a key milestone towards the development of future polarization-engineered oxide heterostructures embedded in quasi-1d nanodevices.

1. Introduction

Zinc oxide is a wide-band (3.37 eV) wurtzite semiconductor which is polar in the [0001] direction. This polarity makes it a candidate material for polarization engineered heterostructures [1,2] and piezoelectric applications [3]. In quasi one-dimensional (1d) polar nanostructures the mutual orientation of the polar and long axes of the nanostructure determines possible device geometries which exploit polarization. ZnO nanowires grow along the polar [0001] axis [4,5] (*i.e.* with the polar and long axes parallel). 1d ZnO nanostructures with long axes other than [0001] (nanobelts due to rectangular cross section [5–7]) have been reported elsewhere and expand the possible applications exploiting polarization. These nanobelts were synthesized in furnaces from precursor ZnO powders [6–9] and hydrothermally [10].

Here we report the growth and morphology control of nanobelts by Molecular Beam Epitaxy (MBE). These nanobelts grow along the non-polar $[1\bar{1}00]$ axis and have side faces which are the polar (0001) facet or only marginally misaligned from this facet. MBE is the tool of choice for the growth of abrupt heteroepitaxial interfaces. (Such interfaces have been demonstrated by MBE in nanowires [11–13]). Therefore an exciting possible application of these nanobelts is the incorporation of two dimensional electron gases (2DEGs) along the long axis of a 1d nanostructure where the 2DEG forms due to the polarity mismatch at abrupt heterointerfaces [14].

2. Experimental

ZnO nanobelts were grown by gold-catalysed plasma-assisted MBE similar to previously reported growth of nanowires [15]. A ~3 nm gold film is evaporated onto **r**-plane $(1\bar{1}02)$ sapphire and heated in-situ forming ~20 nm nanoparticles on the sapphire. Once the growth temperature is reached, 300 W RF oxygen plasma (8×10^{-5} Torr) and zinc flux ($\sim 3.5 \times 10^{-7}$ Torr) are directed at the substrate for two hours.

Nanobelts were characterized by helium ion microscope (HIM), X-ray diffraction (XRD), and high-resolution transmission electron microscope (HRTEM). XRD (Rigaku SmartLab) was performed using Cu K_α emission with a wavelength of 1.54 Å. The HIM (Carl Zeiss Orion NanoFab) was operated with an electron flood gun for charge compensation. TEM (aberration-corrected FEI Titan) was operated at 300 kV.

3. Results and discussion

Nanobelts grown on **r**-plane sapphire predominately grow tilted to the substrate in two directions (arrows in Fig. 1). The growth direction is determined by epitaxial relations of ZnO and the

* Corresponding author at: London Centre for Nanotechnology, 17-19 Gordon Street, London, WC1H 0AH, United Kingdom.
E-mail addresses: oscar.kennedy.14@ucl.ac.uk (O.W. Kennedy), p.warburton@ucl.ac.uk (P.A. Warburton).

https://doi.org/10.1016/j.matlet.2017.10.017
0167-577X/

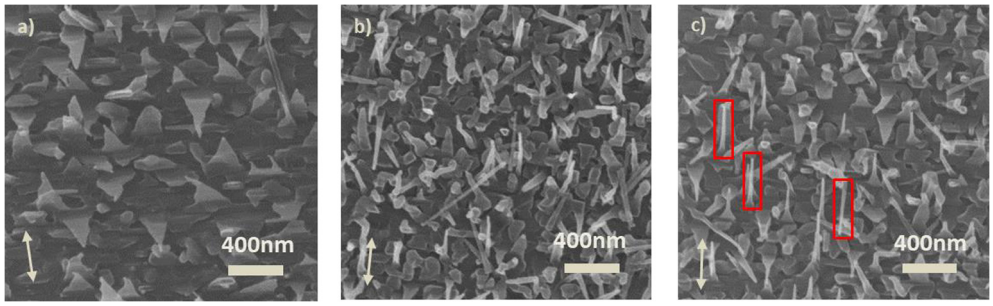

Fig. 1. Normal incidence HIM images of nanobelts grown at (a) 750 °C (b) 800 °C and (c) 890 °C. (c) Nanobelts with significantly reduced tapering are highlighted by red boxes. Arrows are a guide to the eye showing growth directions of nanobelts. (For interpretation of the references to colour in this figure legend, the reader is referred to the web version of this article.)

sapphire substrate and has the two-fold rotational symmetry of the sapphire substrate. There are additionally a small number of 1d nanostructures which do not grow along one of these two directions.

Nanobelt morphology changes with growth temperature. At a lower growth temperature of 750 °C (Fig. 1(a)) the nanobelts are tapered, forming triangles similar to those previously grown on **a**-plane sapphire by PLD [16]. As the growth temperature increases tapering decreases and is significantly reduced at 800 °C (Fig. 1(b)). At the maximum achievable temperature 890 °C (determined by the MBE), a significant fraction of the nanobelts (indicated by the red boxes in Fig. 1(c)) show almost no tapering. Tapering in quasi one-dimensional oxide nanostructures occurs due to side-wall growth [17–19] which is suppressed at increased growth temperature. Sidewall growth in 1d oxide nanostructures is caused by the reaction of surface adsorbed species as they diffuse up the sidewalls of the nanostructure [18], so we attribute suppression of the sidewall growth to the reduced surface adsorption of reactants due to the higher growth temperature. Comparing XRD pole figures (Fig. SI1), confirms that only morphology changes with temperature and that the crystallographic orientation of the nanobelts doesn't change.

Tilting in the HIM reveals the three-dimensional morphology and growth direction of the nanobelts. Tilting to 40° allows a side view of the nanobelts (Fig. 2(a)) which shows their morphology – triangular lamellae for those grown at low temperatures (750 °C). Crystallographic directions (determined later in this paper) have been labelled in the schematic in Fig. 2(a); the face labelled [0001] is the polar face and the face labelled [11$\bar{2}$0] the non-polar face. The triangular lamellar morphology results from the combination of sidewall and catalysed axial growth mechanisms. Sidewall growth occurs preferentially on the polar face due to the energy cost associated with exposed polar faces. Island nucleation on polar faces does not increase the amount of exposed polar face (unlike nucleation on non-polar faces). The ratio of the rates of sidewall growth and axial growth determine the degree of tapering.

Tilting about a different axis to ±31° brings one of the two dominant nanobelt growth directions parallel to the incident He-ion beam of the HIM as shown in Fig. 2(b, c). It is possible to distinguish nanobelts aligned parallel to the incident He-ions from other nanostructures – the former appear bright. This contrast enhancement is due to increased secondary electron emission from the side faces of the narrow triangular lamellae as the ion beam penetrates the nanobelt. These images show that the nanobelts have a rectangular cross section with thickness 20–30 nm.

Low magnification TEM images (inset to Fig. 3(a)) show the shape of a nanobelt. Higher magnification HRTEM (Fig. 3(a)) resolve crystal planes within a nanobelt. From the FFT of HRTEM images it is determined that these nanobelts grow along [1$\bar{1}$00] (Fig. 3(a)) with [0001] perpendicular to the growth direction as labelled in the inset to Fig. 2(a). The nanobelts are not single crystals, instead showing planar defects perpendicular to the [0001] direction. These defects have been widely reported in nanobelts [4,6,20] growing along [1$\bar{1}$00] and are the Wurtzite I_2 basal plane stacking fault [20].

XRD pole figures were collected by aligning the diffractometer to Bragg peaks corresponding to nanobelt axes determined by TEM. By aligning the diffractometer to the (1$\bar{1}$00) Bragg peak (*i.e.* the growth axis of nanobelts), the distribution of growth directions was mapped (Fig. 3(b)). This pole figure has two peaks 180° separated in φ, consistent with the HIM (nanobelts grow along one axis at an angle of ~31°) and the TEM (the nanobelt growth axis is [1$\bar{1}$00]). A schematic of the sample orientation at these peaks is shown in Fig. 3(d).

The (0002) pole figure (Fig. 3(c)) has two intense peaks at χ = 90°, i.e. on the outer edge of the pole figure. These peaks are 90°

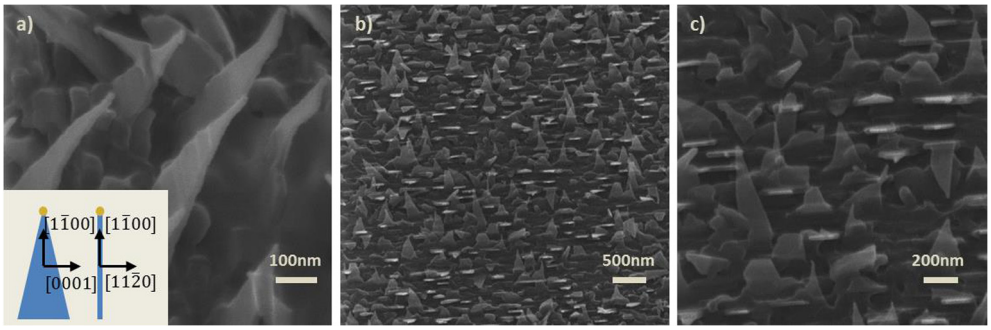

Fig. 2. HIM images of nanobelts grown at 750 °C. Images are taken at (a) 40° and (b, c) 31° tilt showing nanobelt morphology and growth direction relative to the substrate. The tilt axis in (a) is perpendicular to that in (b, c). In (a), projections of the nanobelts from two perpendicular directions are shown as an inset with crystallographic directions (as determined by XRD and HRTEM) labelled.

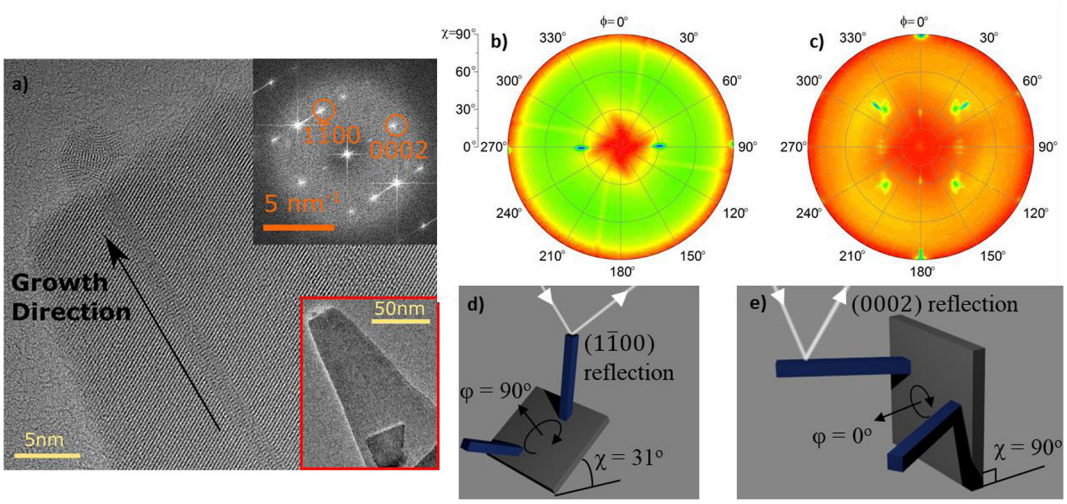

Fig. 3. (a) Representative HRTEM of nanobelt grown at 750 °C. The top inset shows fast Fourier transforms of the HRTEM images with peaks labelled showing both the axial and in plane crystallographic orientations of the nanobelts. The bottom inset shows a lower magnification TEM image showing the nanobelt geometry where some debris covers the bottom of the nanobelt. X-ray diffraction pole figures of ZnO nanobelts grown at 800 °C collected with the diffractometer aligned to (b) the $(1\bar{1}00)$ and (c) the (0002) ZnO Bragg peak. χ changes radially and is 90° at the edge and 0° at the centre. φ changes from 0° to 360° along any line of constant radius. The intensity map is on a logarithmic scale with colours adjusted to maximise contrast in each pole figure, red being the lowest and blue the highest intensity. The resolution in both φ and χ is 1°. (d, e) Schematics of nanobelt orientation for peaks in (b, c). (For interpretation of the references to colour in this figure legend, the reader is referred to the web version of this article.)

misaligned in φ from intense peaks in the $(1\bar{1}00)$ pole figure (Fig. 3 (b)). This is consistent with the HRTEM which shows that [0001] is perpendicular to the direction of growth – Fig. 3(e) is a schematic of the sample orientation at these (0002) peaks. The (0002) pole figure (Fig. 3(c)) has additional split peaks at lower values of χ. These peaks are less intense than the peaks at $\chi = 90°$ despite a drop in diffracted intensity at high values of χ due to defocussing. The dominant growth mode for nanostructures therefore is along $[1\bar{1}00]$ consistent with TEM analysis. The fourfold peaks at $43° < \chi < 53°$ are likely caused by secondary-phase growth of [0001]-oriented nanowires. Mixed-phase growth of $[1\bar{1}00]$ nanostructures and [0001] nanowires by PLD has also been reported [16].

4. Conclusion

We demonstrate the growth of non-polar 1d ZnO nanostructures, referred to as nanobelts, by MBE for the first time. We may control the morphology of these nanostructures by changing their growth temperature, tapering being reduced with increasing temperature. At high temperature these nanostructures are roughly cuboidal and therefore have a pair of side faces very closely aligned to the (0001) facet. This growth technique has possible applications in the growth of high quality heterointerfaces in 1d nanostructures where polarization mismatched interfaces may extend along the length of the nanostructure.

Acknowledgements

This work was supported by EPSRC grant refs. EP/H005544/1, EP/K024701/1 and EP/K035274/1. OWK thanks Carl Zeiss for funding.

Appendix A. Supplementary data

Supplementary data associated with this article can be found, in the online version, at https://doi.org/10.1016/j.matlet.2017.10.017.

Appendix B. Supplementary data

Supplementary data associated with this article can be found, in the online version, at https://doi.org/10.1016/j.matlet.2017.10.017.

References

[1] J. Falson, D. Maryenko, B. Friess, D. Zhang, Y. Kozuka, A. Tsukazaki, J.H. Smet, Nat. Phys. 11 (2015) 347–351.
[2] J. Falson, Y. Kozuka, M. Uchida, J.H. Smet, T. Arima, A. Tsukazaki, M. Kawasaki, Sci. Rep. 6 (2016) 26598.
[3] Z.L. Wang, J. Song, Science 312 (2006) 242–246.
[4] Y. Ding, X.Y. Kong, Z.L. Wang, Phys. Rev. B – Condens. Matter Mater. Phys. 70 (2004) 1–7.
[5] X.Y. Kong, Z.L. Wang, Appl. Phys. Lett. 84 (2004) 975–977.
[6] Z.W. Pan, Z.R. Dai, Z.L. Wang, Science 291 (2001) 1947–1949.
[7] W. Wang, B. Zeng, J. Yang, B. Poudel, J. Huang, M.J. Naughton, Z. Ren, Adv. Mater. 18 (2006) 3275–3278.
[8] C. Ronning, P.X. Gao, Y. Ding, Z.L. Wang, D. Schwen, Appl. Phys. Lett. 84 (2004) 783–785.
[9] Y.B. Li, Y. Bando, T. Sato, K. Kurashima, Appl. Phys. Lett. 81 (2002) 144–146.
[10] Y. Xi, C.G. Hu, X.Y. Han, Y.F. Xiong, P.X. Gao, G.B. Liu, Solid State Commun. 141 (2007) 506–509.
[11] G. Tourbot, C. Bougerol, A. Grenier, M. Den Hertog, D. Sam-Giao, D. Cooper, P. Gilet, B. Gayral, B. Daudin, Nanotechnology 22 (2011) 75601.
[12] S.D. Carnevale, J. Yang, P.J. Phillips, M.J. Mills, R.C. Myers, Nano Lett. 11 (2011) 866–871.
[13] M. Tchernycheva, G.E. Cirlin, G. Patriarche, L. Travers, V. Zwiller, U. Perinetti, J. C. Harmand, Nano Lett. 7 (2007) 1500–1504.
[14] H. Tampo, H. Shibata, K. Maejima, A. Yamada, K. Matsubara, P. Fons, S. Kashiwaya, S. Niki, Y. Chiba, T. Wakamatsu, H. Kanie, Appl. Phys. Lett. 93 (2008) 202104.
[15] I. Isakov, M. Panfilova, M.J.L. Sourribes, P.A. Warburton, Phys. Status Solidi 1313 (2013).
[16] C. Weigand, J. Tveit, C. Ladam, R. Holmestad, J. Grepstad, H. Weman, J. Cryst. Growth 355 (2012) 52–58.
[17] K. Nagashima, T. Yanagida, H. Tanaka, T. Kawai, Appl. Phys. Lett. 90 (2007).
[18] K. Nagashima, T. Yanagida, K. Oka, H. Tanaka, T. Kawai, Appl. Phys. Lett. 93 (2008) 91–94.
[19] T. Terasako, T. Fujiwara, M. Yagi, S. Shirakata, Jpn. J. Appl. Phys. 50 (2011).
[20] Y. Ding, Z.L. Wang, Micron 40 (2009) 335–342.